International Journal of Nanomedicine

Dovepress
open access to scientific and medical research

Open Access Full Text Article

ORIGINAL RESEARCH

Anti-Metastatic Effect of Gold Nanoparticle-Conjugated *Maclura tricuspidata* Extract on Human Hepatocellular Carcinoma Cells

This article was published in the following Dove Press journal:
International Journal of Nanomedicine

Sun Young Park[1]
Beomjin Kim[2]
Zhengwei Cui[3]
Geuntae Park[4]
Young-Whan Choi[3]

[1]Bio-IT Fusion Technology Research Institute, Pusan National University, Busan 609-735, Korea; [2]Department of Nanomaterials Engineering, Pusan National University, Busan 609-735, Korea; [3]Department of Horticultural Bioscience, Pusan National University, Myrang 627-706, Korea; [4]Department of Nanofusion Technology, Graduate School, Pusan National University, Busan, 609-735, Korea

Correspondence: Geuntae Park
Department of Nanofusion Technology, Graduate School, Pusan National University, Busan 609-735, Republic of Korea
Tel +82-51-510-3740
Fax +82-51-518-4113
Email gtpark@pusan.ac.kr

Young-Whan Choi
Department of Horticultural Bioscience, Pusan National University, Miryang 627-706, Republic of Korea
Tel +82-55-350-5522
Fax +82-55-350-5529
Email ywchoi@pusan.ac.kr

Purpose: We aimed to study green-synthesized gold nanoparticles (GNPs) from *Maclura tricuspidata* (MT) root (MTR), stem (MTS), leaf (MTL), and fruit (MTF) extracts and evaluate their anti-metastatic properties in hepatocellular carcinoma cells. *Maclura tricuspidata* belongs to the Moraceae family and is widely used as a traditional medicinal plant given its biological activities.

Methods: We quantified the phenolic and flavonoid contents, reducing capacity, and antioxidant activity of all four extracts. The facile and optimum synthesis of MT-GNPs was visualized using UV-vis spectra and dynamic light scattering (DLS). Surface morphology, selected area electron diffraction (SAED), and fast Fourier transform (FFT) pattern of MT-GNPs were assessed using high-resolution transmission electron microscopy (HR-TEM). The crystallized gold pattern of MT-GNPs was evaluated using energy dispersive spectroscopy (EDS) and X-ray diffraction (XRD). The functionalizing ligands of MT-extracts and MT-GNPs were determined using Fourier-transform infrared spectroscopy (FT-IR). The photocatalytic capabilities of MT-GNPs were assessed by measuring the reduction of rhodamine B and methylene blue. Cell viability assay was detected using Cell Counting Kit-8 solution. Anti-migratory and anti-invasive effects were assessed using cell migration and invasion assays. Matrix metalloproteinase (MMP)-9 and phospholipase D (PLD) enzymatic activities were measured using gelatin zymography and Amplex Red PLD assay, respectively. Western blotting and luciferase assay were used to detect protein expression.

Results: All extracts had high phenolic and flavonoid contents and strong antioxidant and reducing capacities. Results from UV-Vis spectra, DLS, HR-TEM, EDS, XRD, and FT-IR showed the successful formation of MT-GNP with surface morphology, crystallinity, reduction capacity, capsulation, and stabilization. MTR-GNPs and MTS-GNPs had better catalytic activities than MTL-GNPs and MTF-GNPs for reduction of methylene blue and rhodamine B. Moreover, MTS-GNPs and MTR-GNPs exhibited the highest anti-migratory and anti-invasive potential and seemed to be more biologically active than the MTS and MTR extracts. Treatment with MT-GNPs decreased the enzymatic activity, translation levels of MMP-9 and PLD1. Our results showed that MTS-GNPs and MTR-GNPs could dramatically reverse transforming growth factor-β-induced vimentin and N-cadherin upregulation and E-cadherin downregulation.

Conclusion: The application of GNPs as a potential treatment approach for hepatocellular carcinoma can improve therapeutic efficiency.

Keywords: MT-GNPs, *Maclura tricuspidata*, hepatocellular carcinoma cells, epithelial–mesenchymal transition

Introduction

Over the last decade, rapid green synthesis methodologies and approaches for producing gold nanoparticles (GNPs) have been an interesting area in nanobiotechnology.

Currently, GNP-mediated biogenic sources that are chosen to substitute toxic chemical methods have shown great potential in biomedical, pharmaceutical, and industrial fields.[1,2] The green synthesis of GNPs is beneficial over chemical and physical methods as it is low-cost, sustainable, eco-friendly, reliable, and can be without difficulty scaled up. These methods also prevent the production of undesirable or hazardous by-products. The green synthesis of GNPs involves exploitation of phytochemical characteristics, such as reducing capacity, stabilization, and capping biogenic sources.[3,4] GNPs are noteworthy owing to their extensive applications in cosmetics, biomedical, food, and health industries. This may be because of their unique conductivity, optical catalytic activity, biocompatible nature, and better structural properties than their bulk counterparts. Several studies have revealed certain molecular mechanisms underlying the anticancer effects of green-synthesized GNPs. GNPs can also act by targeting various molecular factors for hallmark cancer events, such as cancer angiogenesis, progression, and metastasis.[5–7] In the field of biomedicine, GNPs can be used for efficient approaches, such as drug delivery vehicles and agents for the treatment of cancer. Nanomedical studies have also recommended that GNPs, particularly biocompatible GNPs, may have advantageous roles in inhibiting tumor progression, suggesting that GNPs could be possibly used for the chemoprevention of cancer.[8–10] However, studies reporting the anti-metastatic effects of GNPs are relatively limited.

Tumor metastasis is the major trigger of high death rates in cancer patients and poses a significant challenge in cancer treatment due to its complexity and the multiple steps involved. Metastasis is responsible for approximately 90% of all cancer-related mortality due to the breadth of principal tumor cells to distant tissues, developing secondary tumors, which cannot be removed by chemotherapy in conservative treatment.[11,12] Hepatocellular carcinoma is already the third leading cause of cancer-associated mortality which is considered by high morbidity and mortality because of metastasis-induced malignancy.[13,14] Therefore, extensive efforts are needed to identify novel therapeutic agents and inhibit the metastatic process in order to develop successful long-term treatments.

Epithelial–mesenchymal transition (EMT) is the key initiating step in the progression of hepatic malignancies. During EMT, hepatocellular carcinoma cells lose their epithelial characteristics and the expression of intercellular adhesion molecules, such as E-cadherin and ZO-1, is declined, while that of mesenchymal indicators, such as N-cadherin, vimentin, and fibronectin, is increased, which in turn enhances the invasive migration and metastatic capacities of these cells.[15] The tumor suppressor E-cadherin shows a strategic role in preventing metastasis, and a switch from E-cadherin to N-cadherin expression is routinely investigated to monitor EMT during hepatic malignancies. The expression of these EMT markers, especially E-cadherin, is controlled by numerous transcription factors, such as Twist, Slug, and Snail.[16] These transcription factors also regulate the transcription and translation of matrix metalloproteinases (MMPs), which play a definitive action in hepatic malignancies via stimulation of the EMT signaling pathway. In particular, MMP-9 is a type of zinc-dependent protease that plays a critical action in metastasis through the degradation of the extracellular matrix. Furthermore, it can break down the basement membrane, enabling hepatocellular carcinoma cells to migrate and invade the surrounding cells, thus leading to cancer progression.[17] Transforming growth factor-β (TGF-β) is one of the most potent EMT inducers and a pleiotropic cytokine that promotes metastasis of hepatocellular carcinoma cells. EMT is regulated by numerous signaling pathways from the tumor microenvironment, including various receptor-associated signaling enzymes.[18] Phospholipase D (PLD) shows a critical action in the modulation of a wide range of cellular as well as pathological processes, including tumor proliferation, migration, invasion and metastasis. PLD is activated extensively by various oncogenes including v-Raf, v-Ras and v-Src, and hence, it is currently one of the major molecular targets for the treatment of several cancers including pancreatic, breast, lung, gastric, and liver cancers.[19–21]

The water-soluble organic moieties of medicinal plants play an important role in the green synthesis of GNPs using phytochemicals with significant antioxidant properties.[3] Medicinal plant-based GNPs have been thoroughly analyzed, and it has been experimentally acknowledged that they exhibit medicinal treatments as well as biological properties, such as anti-bacterial, anti-inflammatory, anti-oxidative, and anti-cancer activities.[22–25] *Maclura tricuspidata* (MT) is a member of the Moraceae family and is distributed in Korea and East Asia. Different parts of MT including its roots, stems, leaves, and fruit have been widely used for medicinal purposes to treat conditions such as tumors, liver damage, jaundice, chronic gastritis, rheumatism, as well as external and internal hemorrhage. The pharmacological effects of the roots (MTR), stems (MTS), leaves (MTL), fruits (MTS) of MT are owing to the presence of high phenolic compounds,

flavonoids, diterpenoids, terpenoids, and alkaloids. In particular, phenolic compounds, like cudratricusxanthones, cudraxanthones, and 1,3,7-trihydroxy-4-(1,1-dimethyl-2-propenyl)-5,6-(2,2-dimethylchromeno)xanthone have antioxidant, anti-bacterial, anti-inflammatory and anti-cancer characteristics.[26–29] The results of the present study demonstrated that the preparation of GNPs from MTR, MTS, MTF, and MTL extracts is more beneficial than using conventional methods as they contain high phenolic compounds, which are accountable for the reduction, encapsulation, and stabilization of GNPs. The extracts from the different parts of MT contain high levels of phenolic and flavonoid compounds, and hence, have high radical-scavenging and reducing activities, which are important properties for green-synthesized MT-GNPs. This is the first detailed study on the assessment of the physicochemical characteristics and anti-metastatic properties of different MT-GNPs (MTR-GNPs, MTS-GNPs, MTL-GNPs, and MTF-GNPs), synthesized from different parts of MT, in human hepatocellular carcinoma cells.

Materials and Methods

Reagents

All reagents, including 2,2′-azino-bis(3-ethylbenzothiazoline-6-sulphonic acid) (ABTS), methylene blue, chloroauric acid ($HAuCl_4 \cdot 3H_2O$), rhodamine B, dimethyl sulfoxide (DMSO), 2,2-diphenyl-1-picrylhydrazyl (DPPH) and other chemicals were obtained from Sigma-Aldrich (St. Louis, MO, USA). Antibodies against MMP-9, N-cadherin, PLD-1, E-cadherin, α-tubulin, and vimentin were acquired from Cell Signaling Technology, Inc. (Beverly, MA, USA). All other chemicals indicated were of analytical reagent grade.

Preparation of MT Extracts

MT samples were composed from Miryang, Gyungnam Province, Korea, in December 2018. The botanical identification was prepared by Dr. Young Whan Choi, and a voucher specimen (No. MT20180011) was placed at the laboratory of the Natural Products Research Lab., College of Natural Resources and Bioscience, Pusan National University, Korea. Briefly, the roots, stems, leaves, and fruits of MT were powdered with an electric mixer (HMF-3100S; Hanil Electric, Seoul, Korea), subsequently being dried in a hot-air drying machine (JSR, Seoul, Korea) for 24 h at 60 °C. The dried roots, stems, leaves, and fruits (30 g) of MT were then extracted with double-distilled water at 100 °C for 4 h, filtered, and concentrated with a rotary vacuum evaporator (Buchi Rotavapor R-14; Buchi Labortechnik, Flawil, Switzerland) to acquire 5.467, 2.000, 8.867, and 2.711 g, respectively. The MT extracts (MTR, MTS, MTL, and MTF) were liquefied in double-distilled water, stored as 50 mg/mL stock solutions at 4 °C, and diluted to the chosen concentration using the GNPs medium.

Total Phenolic and Flavonoid Content of MT Extracts

The total phenolic and flavonoid contents of MT extracts (MTR, MTS, MTL, and MTF) were determined using the Folin–Ciocalteu and aluminum chloride colorimetric methods, as described previously.[30] The total phenolic and flavonoid content was expressed as gallic acid equivalent (GAE) per g and quercetin equivalent (OE) per g of MT extracts (MTR, MTS, MTL, and MTF).

DPPH and ABTS Assay to Study the Free Radical Scavenging Capacity of MT Extracts

The DPPH and ABTS radical scavenging activities of MT extracts (MTR, MTS, MTL, and MTF) were determined according to a previously described method,[30] with slight modifications. MT extracts (MTR, MTS, MTL, and MTF) were mixed with DPPH solution (60 μM) or ABTS solution (7 mM) in microplates. The samples were shaken vigorously and then kept in the dark at 25°C for 2 h. The optical density of the mixture was measured at 510 nm or 734 nm.

Determination of the Reducing Potential of MT Extracts

The reducing potential of MT extracts (MTR, MTS, MTL, and MTF) was determined according to a previously described method,[30] with slight alterations. The absorbance was quantified at 700 nm with a spectrophotometer (Evolution™ 300 UV-Vis Spectrophotometer, Thermo Fisher Scientific).

Synthesis and Physicochemical Characterization of MT-GNPs

For the reduction of $HAuCl_4$ to GNPs, 1 mM of aqueous $HAuCl_4$ solution was mixed with MT extracts (MTR, MTS, MTL, and MTF), respectively. The mixture was incubated at 25°C for 15 min, and the color changed from yellow to violet after 15 min, which confirmed the formation of GNPs. The formation of MTR-, MTS-, MTL- and MTF-GNPs was

detected using an Evolution 300 UV-Vis absorption Spectrophotometer (Thermo Fisher Scientific) from 300 to 800 nm. The particle size, zeta-potential, and polydispersity index (PDI) of MTR-, MTS-, MTL- and MTF-GNPs were determined at 25 °C by DLS technique using Zetasizer Nano ZS90 (Malvern Instruments, Malvern, UK). The MTR-, MTS-, MTL- and MTF-GNPs were placed in a disposable zeta cell at 25 °C. Distilled water was used as a reference for the dispersing buffer. The results are given as the average particle size, zeta-potential, and PDI acquired from the examination of three different batches, each of them measured three times. The XRD patterns were collected using a X'Pert 3 Powder X-ray Diffractometer (Malvern Panalytical, Malvern, UK) operating at a 30 to 80 s scanning range, 40 kV voltage, and 30 mA current. The FT-IR patterns were collected using a Perkin Elmer Spectrum GX FT-IR Spectrophotometer with KBr pellets operating at a range of 400 to 4000 cm−1. To determine the surface morphology, crystallinity, and chemical composition of MTR-, MTS-, MTL- and MTF-GNPs, one drop of the reaction mixture was deposited on the copper grid and then the MTR-, MTS-, MTL- and MTF-GNPs were dried completely. The HR-TEM operating at a 200 KV accelerated voltage as well as the selected area electron diffraction (SAED), fast Fourier transform (FFT), high-angle annular dark field (HAADF), and EDS measurements were conducted on the Thermo Scientific (FEI) Talos F200X G2 TEM instrument.

Photocatalytic Activities of MT-GNPs

The photocatalytic activities of the MTR-, MTS-, MTL-, and MTF-GNPs were evaluated based on the degradation of methylene blue and rhodamine B dyes, as previously described.[5] In brief, solution of 0.8 mM methylene blue and 0.05 mM rhodamine B solution were added to MTR-, MTS-, MTL-, and MTF-GNPs, following which an ice-cold solution of 0.06 M sodium borohydride was supplementary. The degradation of methylene blue and rhodamine B was measured on a wavelength range of 300–800 nm with regular intervals (1 min).

Cell Culture and Cell Viability

Human hepatocellular carcinoma cell lines (HepG2 and SK-Hep-1) were acquired from American Type Culture Collection (ATCC, Manassas, VA, USA). HepG2 and SK-Hep-1 Cells were incubated in Eagle's minimum essential medium (EMEM) added with 1% penicillin/streptomycin and 10% fetal bovine serum (Gibco; Thermo Fisher Scientific, Waltham, MA, USA). All cells were incubated and treated at 37°C with 5% CO_2 and passaged in 3 days. Cells were cultured in 24-well plates at a density of 3×10^4 cells per well for 24 h. Cells were treated with various concentrations (0–100 μg/mL) of MTR, MTS, MTL, and MTF and MTR-, MTS-, MTL-, and MTF-GNPs and incubated at 37 °C with 5% CO2 for 24 h, 48 h, and 72 h. Afterward, the CCK-8 solution was treated to the medium at 37 °C with 5% CO2 for 4 h. The optical density was read at a wavelength of 450 nm.

Cell Migration and Transwell Invasion Assay

The influence of MT-GNPs on the horizontal migration of HepG2 and SK-Hep-1 cells was assessed with the Radius 24-Well Cell Migration Assay (Cell Biolabs, San Diego, CA, USA) according to the manufacturer's guidelines. Images were captured with an inverted microscope at predetermined times (0 and 24 h). Cell migration and invasion were assessed with the CytoSelect 24-Well Cell Migration and Invasion Assay (8 μm; Cell Biolabs, San Diego, CA, USA) according to the manufacturer's specifications. HepG2 and SK-Hep-1 cells that infiltrated to the bottom surface were stained using crystal violet (for about 5 min) for visualization.

Gelatin Zymography

MMP-9 activity was assessed using the Zymogram-PAG System kit (Koma Biotech, Seoul, Korea) according to the manufacturer's specifications. Briefly, the culture media of HepG2 and SK-Hep-1 cell were mixed with Zymogram sample buffer (2X) and acceptable to stand for 10 min at 25 °C. After electrophoresis (125 V constant, 90 min) with Zymogram running buffer (1X), the gels were washed with Zymogram renaturing buffer (1X) for 30 min at 25 °C and then incubated for 16 h at 37°C with Zymogram developing buffer (1X). The gels were stained with Coomassie Brilliant Blue R-250 for 30 min, and then de-stained using the Coomassie R-250 destain (Bio-Rad, CA, USA).

PLD Activity Assay

PLD activity was analyzed using the Amplex Red Phospholipase D Assay Kit (Molecular Probes) by spectrofluorimetry, according to the manufacturer's specifications. In brief, HepG2 and SK-Hep-1 cells were trypsinized and centrifuged to remove the supernatant. Subsequently, cell pellets were added in the Amplex Red reaction buffer in the kit, vortex vigorously and incubated on ice for 5 min, then centrifuged. PLD enzymatic activity

was measured on a FLUOsta0r Omega Plate Reader (BMG Labtech). Each sample is normalized against the protein concentration of the sample.

Western Blotting

The quantitative samples were loaded into the 10% SDS-PAGE and separated by electrophoresis. Then, transferred to PVDF membrane (Amersham Biosciences, Piscataway, NJ, USA). Took out the membranes and blocked with 5% BSA for 1 h at room temperature, the PVDF membranes were incubated with the following primary antibodies: Anti-MMP-9, anti-PLD1, anti-E-cadherin, anti-N-cadherin, anti-vimentin and anti-α-tubulin (Cell Signaling, Waltham, MA, USA). After washing three times for 10 min with Tris-buffered saline and Tween 20 (TBST), the membranes were incubated with horseradish peroxidase-conjugated secondary antibodies (anti-rabbit IgG, anti-mouse IgG, Cell Signaling, Waltham, MA, USA) for 1 h at room temperature. The protein bands were detected using an enhanced Pierce ECL Western Blotting Substrate (Thermo Fisher Scientific) with an ImageQuant 350 analyzer (Amersham Biosciences).

Statistical Analysis

All data are represented as means ± SEM of three independent replicates for each group. Comparisons were conducted using the Statistical Package for the Social Sciences software, version 17.0 (SPSS Inc. Released 2008. SPSS Statistics for Windows, Version 17.0. Chicago: SPSS Inc). Student's *t*-test and one-way analysis of variance (ANOVA) were used to evaluate the differences among groups. A P-value of < 0.01 or < 0.05 was considered to indicate a statistically significant difference.

Results

Optimization of MT-GNPs Using MT Extract as a Green-Reductant

In this present study, GNPs were rapidly synthesized using different MT extracts as green-reductants. To determine the potential effect of MTR, MTS, MTL, and MTF extracts on the reduction, capsulation, and stabilization of GNPs, their total phenolic and flavonoid contents as well as a powerful reducing capacity, and antioxidant (ABTS and DPPH) activities were evaluated. As shown in Table 1, the results of the total phenolic analysis showed that MTR extract had the highest phenolic content followed by MTS and MTL, whereas MTF extract had the lowest phenolic content. Further, we observed that MTR, MTS, MTL, and MTF extracts all had significantly high flavonoid contents (Table 1). The MTS extract (12.9 ± 1.9 mg AAE/g) was found to exhibit the highest reducing potential, followed by MTR (12.4 ± 0.9 mg AAE/g) and the MTL (9.7 ± 1.4 mg AAE/g) extracts, while MTF extract (6.9 ± 1.5 mg AAE/g) had the lowest reducing potential (Table 1). Moreover, the results of antioxidant activity analyses (Table 1) showed that the radical scavenging activities of MT extracts analyzed using DPPH assay were found to be in the following order: MTR > MTS > MTL > MTF. The radical scavenging activities analyzed using the ABTS assay were found to be in the following order: MTR > MTL > MTS > MTF. In this study, we further assessed the addition of the MTR, MTS, MTL, and MTF extracts to an aqueous solution of $HAuCl_4$ resulted in the formation of GNPs. Addition of an aqueous solution of $HAuCl_4$ to MTR, MTS, MTL, and MTF extracts at room temperature for 15 min resulted in the formation of MTR-GNPs, MTS-GNPs, MTL-GNPs, and MTF-GNPs, respectively. This was apparent from the color alteration of the solution from ivory yellow to purple or red color as well as the absorption peak, λmax, which was observed between 520 and 527 nm when the GNPs were subjected to surface plasmon resonance (Figure 1A). In addition, the MTR-, MTS-, MTL-, and MTF-GNPs were further analyzed by DLS to assess hydrodynamic size distribution, zeta potential, and polydispersity index (PDI). The hydrodynamic size distributions were 89.0 ± 5.21, 88.50 ± 10.16, 91.43 ± 1.87, and 96.60 ± 7.03 nm; the zeta potential values were

Table 1 Antioxidant Capability of MTR, MTS, MTL and MTF Extracts

Plant Parts	Total Phenolic (μg GAE/g)	Flavonoid (μg QE/g)	Reducing Power (μg AAE/g)	DPPH (%)	ABTS (%)
Root	328.0 ± 16.3	138.6 ± 10.1	12.4 ± 0.9	87.0 ± 4.3	89.3 ± 6.2
Stem	233.5 ± 15.8	117.8 ± 7.0	12.9 ± 1.9	84.4 ± 3.4	84.1 ± 5.6
Leaf	131.5 ± 13.9	110.3 ± 11.3	9.7 ± 1.4	77.2 ± 6.6	84.7 ± 6.9
Fruit	77.5 ± 14.0	117.0 ± 16.3	6.9 ± 1.5	47.4 ± 4.9	87.0 ± 4.3

Abbreviations: MTR, *Maclura tricuspidata* root; MTS, *Maclura tricuspidata* stem; MTL, *Maclura tricuspidata* leaves; MTF, *Maclura tricuspidata* fruits; GAE, gallic acid equivalent; QE, quercetin equivalent; AAE, ascorbic acid equivalent; DPPH, 2,2-diphenyl-1-picrylhydrazyl; ABTS, 2,2′-azino-bis (3-ethylbenzothiazoline-6-sulphonic acid).

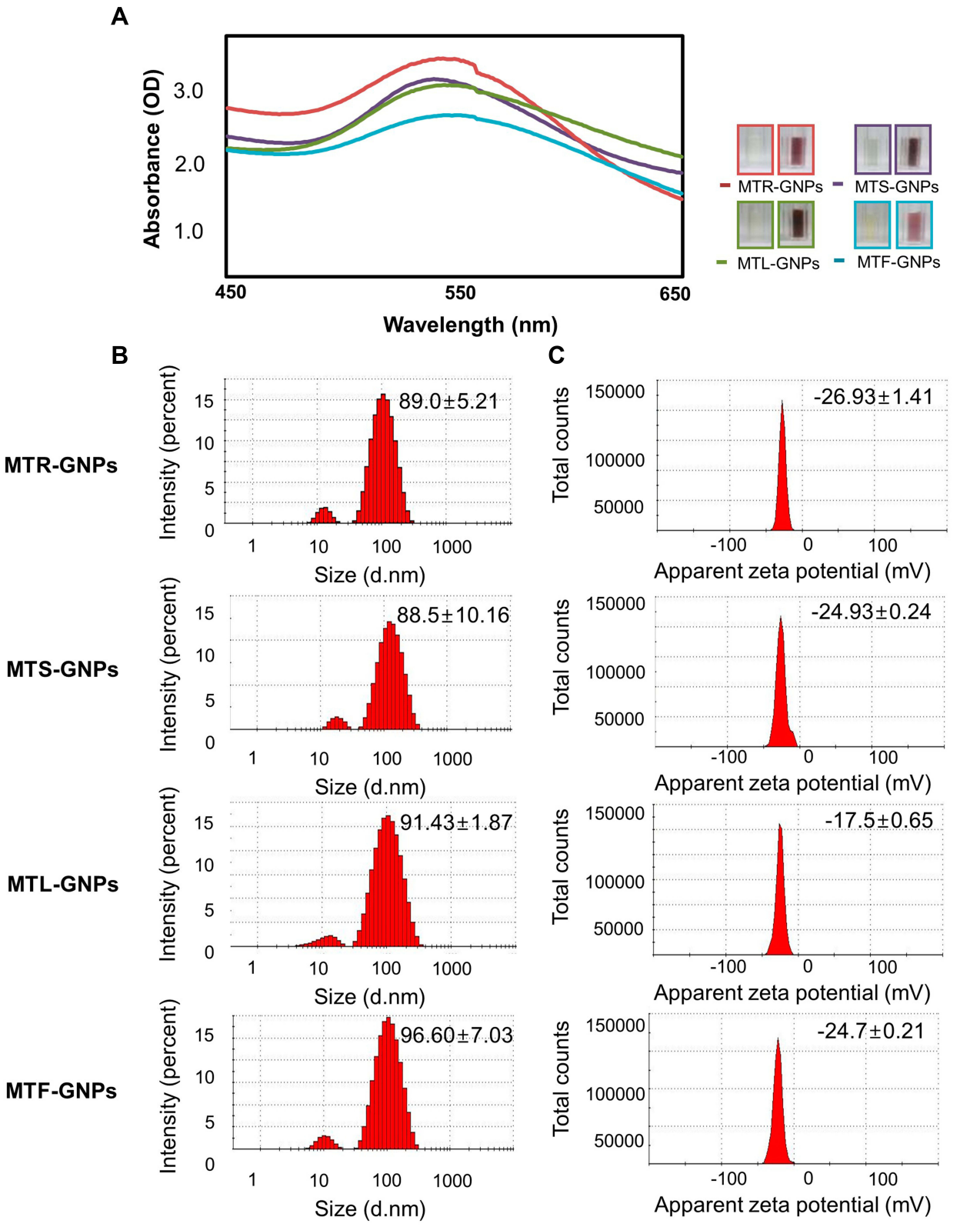

Figure 1 The optimization of MTR-, MTS-, MTL-, and MTF-GNPs.

Notes: (**A**) UV-Vis spectra of MTR-, MTS-, MTL-, and MTF-GNPs. (**B**) The hydrodynamic sizes of MTR-, MTS-, MTL-, and MTF-GNPs were determined by DLS. (**C**) Zeta potential values of MTR-, MTS-, MTL-, and MTF-GNPs were measured by DLS.

Abbreviations: MTR-, MTS-, MTL-, and MTF-GNPs, *Maclura tricuspidata* root-, stem-, leaf-, and fruit-extract-gold nanoparticles, respectively; UV-Vis, ultraviolet-visible; DLS, dynamic light scattering.

–26.93 ± 1.41, –24.93 ± 0.24, –17.50 ± 0.65, and –24.70 ± 0.21 mV; and the PDI values were 0.24 ± 0.01, 0.31 ± 0.02, 0.26 ± 0.02, and 0.32 ± 0.02 for MTR-, MTS-, MTL-, and MTF-GNPs, respectively (Figure 1B and C).

HR-TEM and EDS Studies of MT-GNPs

The surface morphology of MTR-, MTS-, MTL-, and MTF-GNPs was evaluated using HR-TEM. Typical micrographs display GNPs with spherical or hexagonal-shaped morphology, and MTR-, MTS-, MTL-, and MTF-GNPs were able to obtain an average diameter of 23.3 ± 3.7, 25.7 ± 5.3, 24.4 ± 4.3, and 26.3 ± 3.4 nm, respectively (Figure 2A and B). The SAED patterns of MTR-, MTS-, MTL-, and MTF-GNPs also showed a face-centered cubic crystal structure, which was manifested by bright circular spots corresponding to (111), (200), (220), and (311) lattice planes of Bragg's reflection (Figure 2C). The distribution of Au elements in MTR-, MTS-, MTL-, and MTF-GNPs was analyzed using HAADF imaging. Figure 2D indicates a typical red-particle image of the GNPs corresponding to Au element maps. EDS analysis determines the surface chemical composition of the green-synthesized Gold-NPs and results presented three clear Au signals pertaining to the elements in MTR-, MTS-, MTL-, and MTF-GNPs (Figure 2E). Surface plasmon resonance analysis showed that MTR-, MTS-, MTL-, and MTF-GNPs displayed peaks at 0.2–0.4, 2–2.3, and 9.6–9.8 keV, respectively, which was due to the presence of Au.

XRD and FT-IR Studies of MT-GNPs

To examine the well-crystallized gold patterns of MTR-, MTS-, MTL-, and MTF-GNPs, XRD measurements were

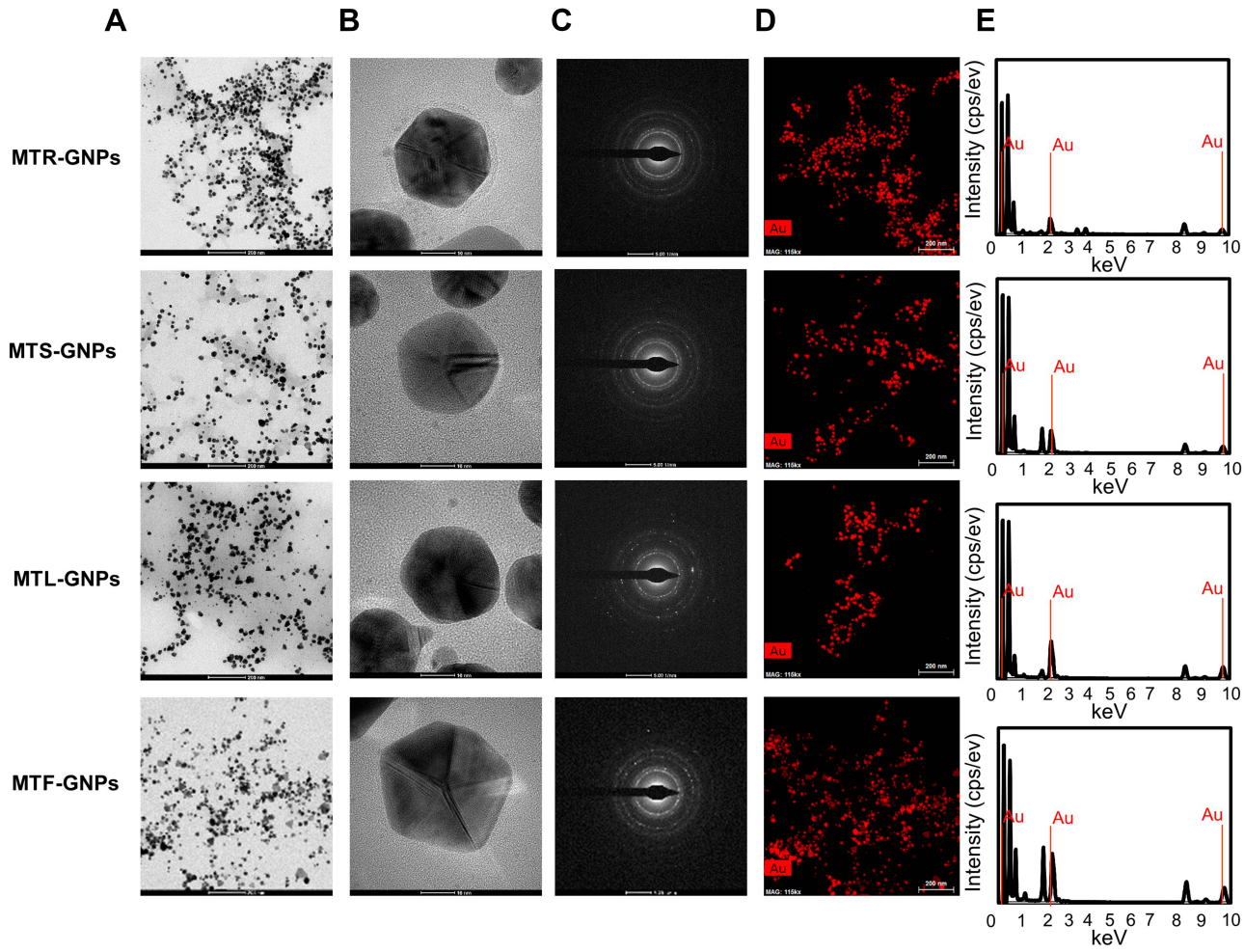

Figure 2 Characterization of MTR-, MTS-, MTL-, and MTF-GNPs.
Notes: HR-TEM images at (**A**) low and (**B**) high magnification, (**C**) SAED patterns, (**D**) HAADF imaging, and (**E**) EDS analysis of MTR-, MTS-, MTL-, and MTF-GNPs.
Abbreviations: HR-TEM, high-resolution transmission electron microscopy; SAED, selected area electron diffraction; HAADF, High-angle annular dark field; EDS, energy dispersive spectroscopy; MTR-, MTS-, MTL-, and MTF-GNPs, *Maclura tricuspidata* root-, stem-, leaf-, and fruit-extract-gold nanoparticles, respectively.

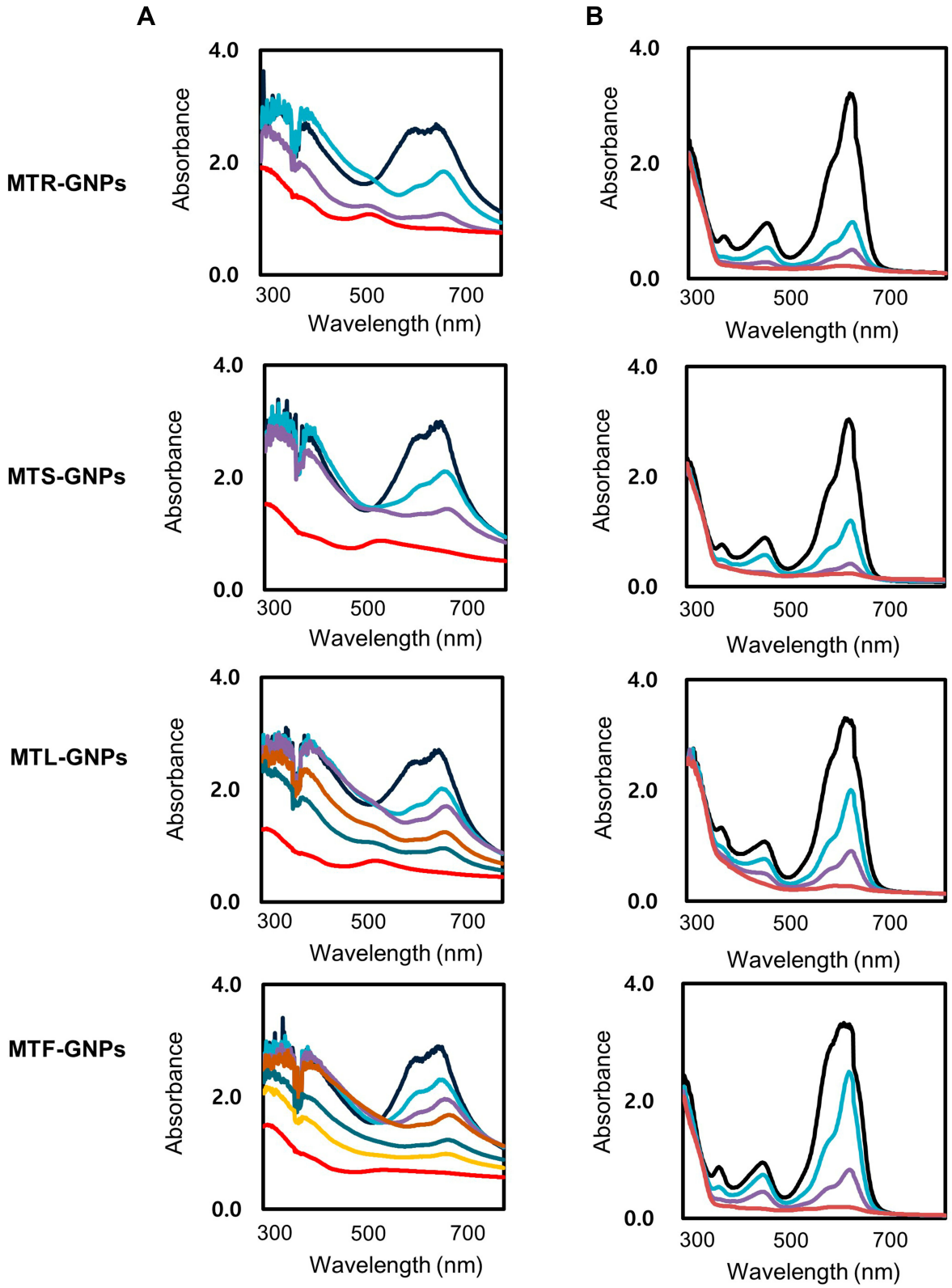

Figure 3 Physicochemical characterization of MTR-, MTS-, MTL-, and MTF-GNPs.
Notes: (**A**) XRD pattern and (**B**) FTIR spectra of MTR-, MTS-, MTL-, and MTF-GNPs.
Abbreviations: XRD, X-ray diffraction; FT-IR, Fourier transform-infrared spectroscopy; MTR-, MTS-, MTL-, and MTF-GNPs, *Maclura tricuspidata* root-, stem-, leaf-, and fruit-extract-gold nanoparticles, respectively.

detailed, as shown in Figure 3A. The main peaks acquired at (111), (200), (220), and (311) corresponded to the Bragg's reflection planes with 2 θ values (30–80°) of 38.18–38.23°, 44.37–44.51°, 64.7–-64.78°, and 77.59–77.85°, respectively. The peak of the XRD spectrum confirmed the presence of elemental and crystalline gold. The "green synthesis" of GNPs involves use of biocompatible materials, which act as functionalizing ligands under physiological conditions, generating GNPs that are more suitable for the biomedical approach. The MT extracts also provide potential functional groups, which get attached to the surface of the MT-GNPs, resulting in capping and stabilization of GNPs. In this study, the FT-IR spectra was analyzed to investigate the existence of bioactive components, such as the capping layer in MT-GNPs. The FT-IR spectra of MT extracts corresponding to MT-GNPs specified high similarity between MT extracts and MT-GNPs. In particular, the prominent peaks of MTR, MTS, MTL, and MTF extracts and their corresponding GNPs were characterized by –OH stretching at 3372.01, 3368.86,

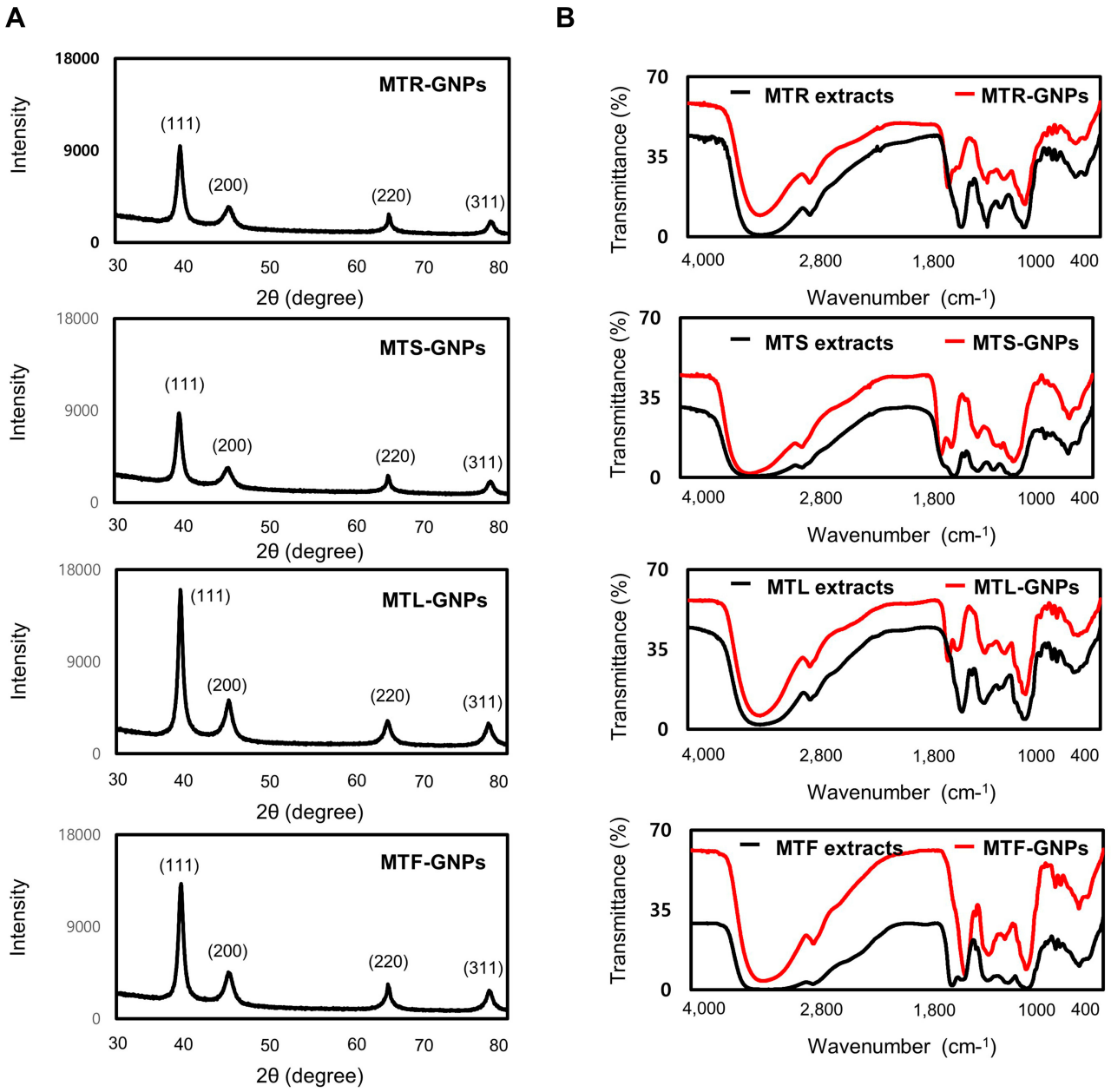

Figure 4 Photocatalytic properties of MTR-, MTS-, MTL-, and MTF-GNPs.
Notes: UV-Vis spectra of (**A**) methylene blue and (**B**) rhodamine B on addition of MTR-, MTS-, MTL-, and MTF-GNPs. Control is non-treated group.
Abbreviations: UV-Vis, ultraviolet-visible; MTR-, MTS-, MTL-, and MTF-GNPs, *Maclura tricuspidata* root-, stem-, leaf-, and fruit-extract-gold nanoparticles, respectively.

3369.05, and 3368.94 cm^{-1}, respectively. In addition, –CH stretching was also observed between 2930.25, 2879.42, 2978.13, and 2960.07 cm^{-1}, respectively, with peaks at 1592.45 (MTR-GNPs) and 1589.52 cm^{-1} (MTS-GNPs) which corresponds to the C-C stretch of aromatic-groups. Moreover, peaks due to C-N stretching were also detected in MTL-GNPs and MTF-GNPs at 1076.25 and 1264.74 cm^{-1}, respectively (Figure 3B). Altogether, these results demonstrated that the reduction, capsulation, and stabilization of MT-GNPs were possibly owing to some functional groups present in the MT extracts, for example, phenols, flavonoids, and proteins.

Photocatalytic Studies of MT-GNPs

The dye degradation of the methylene blue and rhodamine B dyes using sodium borohydride was studied using sodium borohydride in the presence of MTR-, MTS-, MTL-, and MTF-GNPs and monitoring by UV-Vis spectrophotometer. A characteristic absorption peak was identified corresponding to pure methylene blue (665 nm) and rhodamine B (575 nm). In the treatment of MTR-, MTS-, MTL-, and MTF-GNPs as a catalyst, the deep blue (corresponding to methylene blue) and pink-red (corresponding to rhodamine B) color gradually faded and finally disappeared. In Figure 4, the UV-Vis spectra revealed that the addition of all the MTR-, MTS-, MTL-, and MTF-GNPs completely decreased in the wavelength of maximum absorbance within 4–7 min. The catalytic degradation of methylene blue and of rhodamine B by MT-GNPs was found in the following order: MTR-GNPs > MTS-GNPs > MTL-GNPs > MTF-GNPs.

Anti-Migration Studies of MT-GNPs

To examine the effects of MT-GNPs on HepG2 and SK-Hep-1 cell viability, CCK-8 assay was performed using indicated concentrations (0–100 μg/mL) of MT-GNPs for 24, 48, and 72 h. Compared to that in the non-treated control group, cell viability was considerably reduced by MT extract and MT-GNPs at 100 μg/mL doses for 48 and 72 h in HepG2 and SK-Hep-1 cells (Table 2). In contrast, treatment of HepG2 and SK-Hep-1 cells with MTF extract or MTF-GNPs at concentrations of up to 80 μg/mL for 24 h had no effect on cell viability (Table 2). Therefore, HepG2 and SK-Hep-1 cells were treated with MT extract or MT-GNPs at a concentration of 80 μg/mL for 24 h in subsequent experiments. The cell migration assay was performed to assess the ability of MT-GNPs to inhibit tumor cell motility. HepG2 and SK-Hep-1 cells showed high metastatic ability. The cell migration assay showed that the gap was repopulated by the cells. As shown in Figure 5A, the circle-shaped area of the non-treated control group showed no obvious change, while remarkable gap closure was observed in the TGF-β group after an incubation period of 24 h. The ability of MT extracts and MT-GNPs to inhibit migration of treated HepG2 and SK-Hep-1 cells was in the following order:

Table 2 Cell Viability of MTR, MTS, MTL and MTF-GNPs

(mg/mL)	HepG2 (%)			SK-Hep-1 (%)		
	40	80	100	40	80	100
24 h						
MTR-GNP	101.2 ± 0.3	87.9 ± 6.3	69.8 ± 3.1**	94.0 ± 2.2	91.2 ± 2.5	68.9 ± 2.0*
MTS-GNP	98.4 ± 4.5	90.2 ± 1.1	71.9 ± 6.2*	93.2 ± 1.1	83.1 ± 2.3	67.5 ± 2.2**
MTL-GNP	99.1 ± 0.7	100.5 ± 4.0	82.5 ± 2.6**	100.4 ± 1.0	97.2 ± 1.5	86.6 ± 1.5**
MTF-GNP	103.1 ± 0.9	97.5 ± 5.7	79.9 ± 4.7**	100.2 ± 2.2	93.4 ± 2.1	93.2 ± 2.0
48h						
MTR-GNP	77.6 ± 1.5**	75.0 ± 5.4**	48.1 ± 4.7**	73.5 ± 2.5**	63.1 ± 2.0**	49.6 ± 3.7**
MTS-GNP	81.9 ± 2.2*	74.9 ± 1.9**	61.4 ± 6.2**	72.9 ± 3.1**	64.6 ± 0.7**	54.2 ± 2.3**
MTL-GNP	83.0 ± 1.5*	85.8 ± 3.3*	67.1 ± 2.5**	77.1 ± 2.2**	68.1 ± 2.3**	62.4 ± 1.9**
MTF-GNP	88.0 ± 0.8*	77.1 ± 2.6**	71.3 ± 2.2**	77.5 ± 2.6**	68.9 ± 2.5**	62.5 ± 2.0**
72h						
MTR-GNP	61.5 ± 4.0**	55.6 ± 1.5**	27.6 ± 3.1**	63.9 ± 3.0**	54.1 ± 1.1**	34.0 ± 3.8**
MTS-GNP	53.6 ± 2.0**	40.0 ± 0.5**	31.9 ± 2.8**	66.7 ± 2.3**	38.9 ± 2.6**	34.2 ± 4.0**
MTL-GNP	61.0 ± 1.3**	44.7 ± 1.7**	42.9 ± 3.1**	64.5 ± 3.7**	60.2 ± 1.6**	42.5 ± 2.6**
MTF-GNP	65.7 ± 0.4**	59.9 ± 1.6**	52.4 ± 4.6**	62.8 ± 1.5**	62.9 ± 2.2**	53.9 ± 1.1**

Notes: Cell viability of MTR, MTS, MTL and MTF-GNPs were detected by CCK-8 assay. *$p < 0.05$ and **$p < 0.01$ compared to the control group.
Abbreviations: MTR-, MTS-, MTL- and MTF-GNPs, *Maclura tricuspidata* root-, stem-, leaves- and fruits-extract-gold nanoparticles.

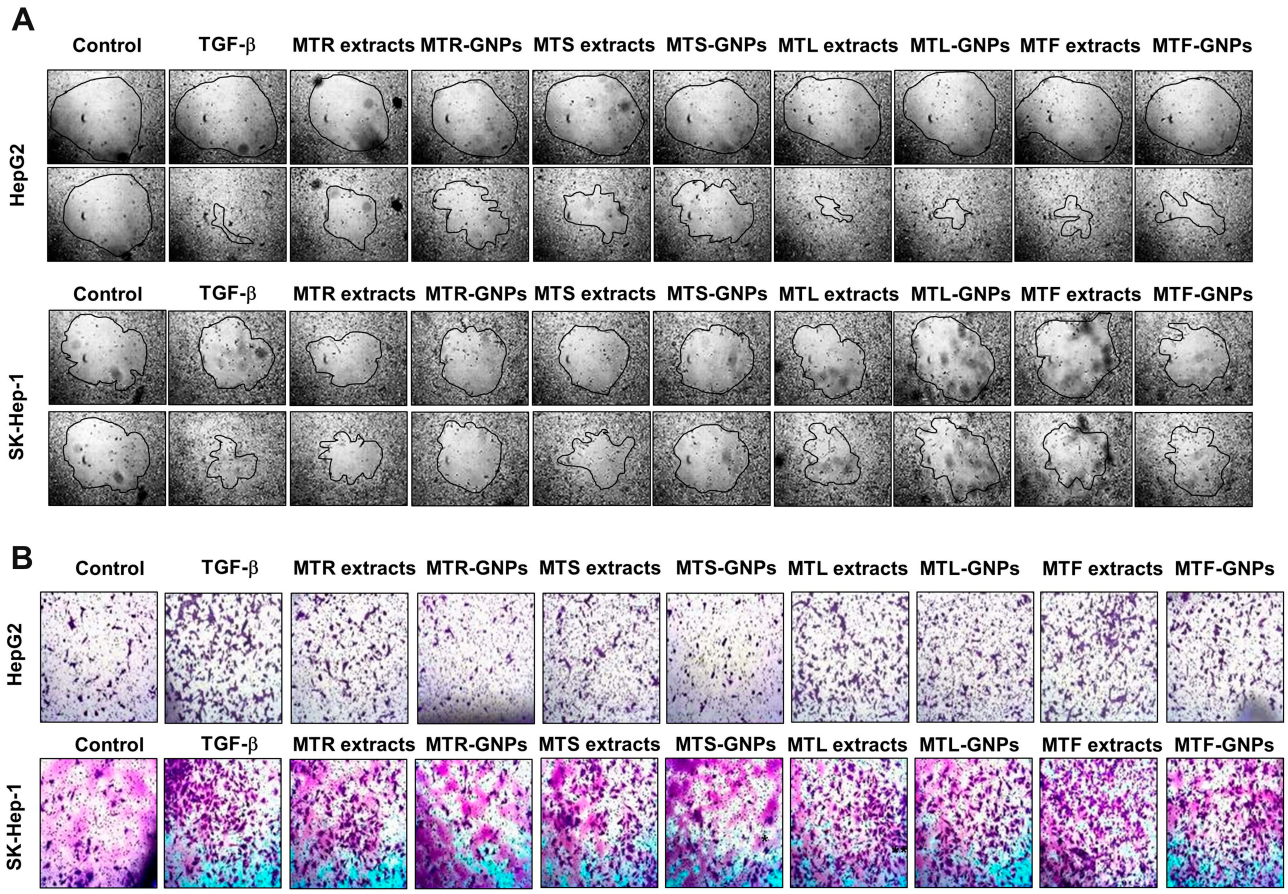

Figure 5 Anti-migration and -invasion effects of MTR-, MTS-, MTL-, and MTF-GNPs.
Notes: (**A**) Cell migration was detected in HepG2 and SK-Hep-1 cells using the Radius™ 24-Well Cell Migration Assay kit. (**B**) Cell invasion was measured with the CytoSelect™ Cell Migration and Invasion assay kit. Control is non-treated group.
Abbreviations: MTR-, MTS-, MTL-, and MTF-GNPs, *Maclura tricuspidata* root-, stem-, leaf-, and fruit-extract-gold nanoparticles, respectively; TGF-β, transforming growth factor-beta.

MTR-GNPs > MTS-GNPs > MTR > MTS > MTL-GNPs > MTF-GNPs > MTL > MTF, indicating that both MTR-GNPs and MTS-GNPs exerted higher inhibitory effects on HepG2 and SK-Hep-1 cell motility compared to other groups (Figure 5A).

Anti-Metastasis Studies of MT-GNPs

Increasing evidence suggests that EMT is the underlying cause of cell invasion and motility in cancer cells.[16] To analyze the inhibition of HepG2 and SK-Hep-1 cell invasion, we performed the transwell assay. The invasion assay results showed that MTR, MTR-GNPs, MTS, MTS-GNPs, MTL, MTL-GNPs, MTF, and MTF-GNPs remarkably decreased cell invasion from 100% to 25.7%, 9.3%, 18.5%, 7.8%, 48.8%, 24.7%, 57.3%, and 35.6%, respectively, in HepG2 cells compared with that in TGF-β-treated cells (Figure 5B). However, the inhibitory effect of MTL, MTL-GNPs, MTF, and MTF-GNPs on cell invasion was not significant in SK-Hep-1 cells compared with that in TGF-β-treated cells. MTR-GNPs and MTS-GNPs showed high invasive abilities as compared to MTL-GNPs and MTF-GNPs in hepatocellular carcinoma cells. Furthermore, we found that the enzymatic activity of MMP-9 was remarkably inhibited by MT-GNPs in TGF-β-treated cells. We used gelatin zymography to further confirm this finding. The results showed that TGF-β-induced MMP-9 enzymatic activity was reversed by MTR, MTR-GNPs, MTS, MTS-GNPs, and MTL-GNPs, but remained unchanged upon treatment with MTL, MTF, and MTF-GNPs. The highest MMP-9 enzymatic activity was seen in the MTS-GNPs group, and the lowest in the MTF-GNPs group (Figure 6A). PLD activity in tumor cells has been confirmed to play a crucial role in tumor metastasis. Consequently, we further examined the effect of MT extracts and MT-GNPs on PLD activity in TGF-β-stimulated HepG2 and SK-Hep-1 cells. These results demonstrated that MTS-GNPs and MTR-GNPs exhibited the highest PLD inhibitory

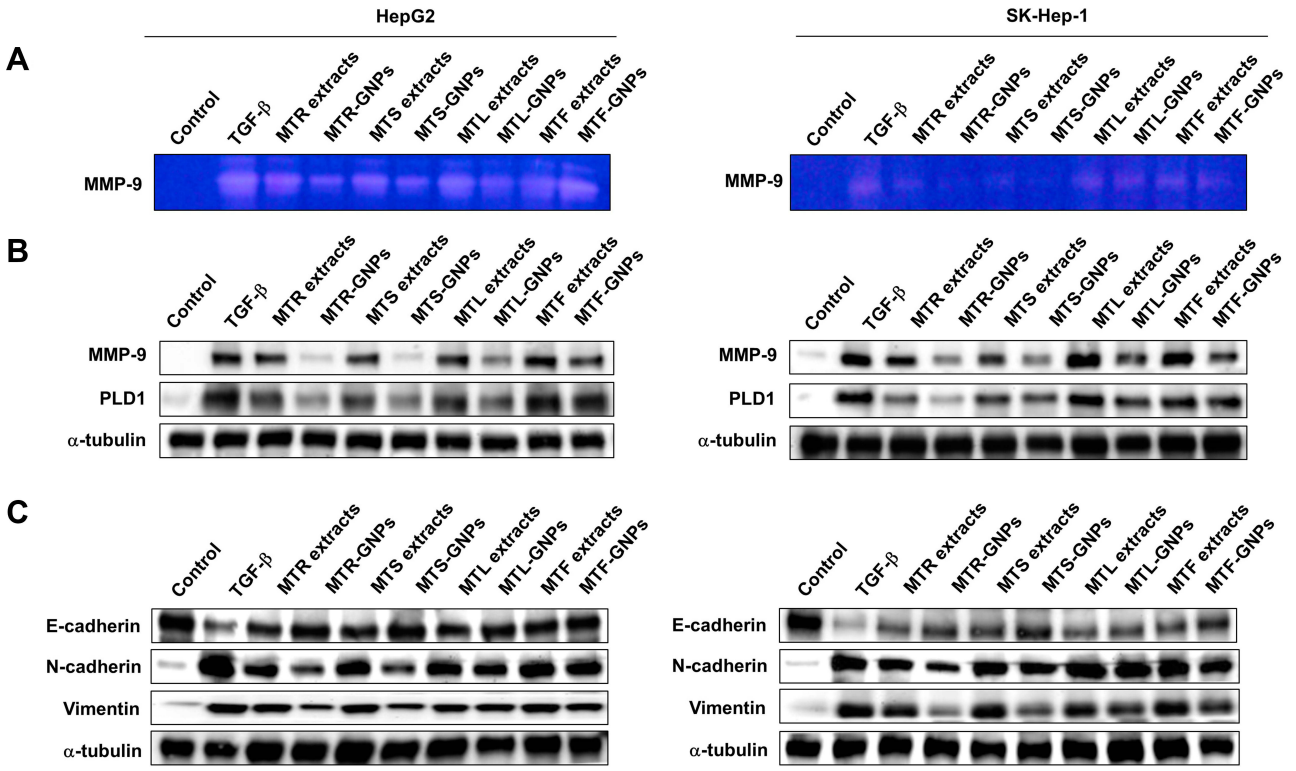

Figure 6 Downregulation of MMP-9, PLD, and other EMT-related proteins by MTR-, MTS-, MTL-, and MTF-GNPs.
Notes: (**A**) MMP-9 enzymatic activity was detected by gelatin zymography. (**B**) Effect of MTR-, MTS-, MTL-, and MTF-GNPs on the expression of MMP-9 and PLD1 proteins. (**C**) Effect of MTR-, MTS-, MTL-, and MTF-GNPs on the protein expression of E-cadherin, N-cadherin, and vimentin. Control is non-treated group.
Abbreviations: MMP-9, matrix metalloproteinase-9; PLD, phospholipase D; TGF-β, transforming growth factor-beta; MTR-, MTS-, MTL-, and MTF-GNPs, *Maclura tricuspidata* root-, stem-, leaf-, and fruit-extract-gold nanoparticles, respectively.

activity, also seemed to be highly active than MTS and MTR extract (Table 3).

Western Blot Analysis of MT-GNPs

Since MMP-9 and PLD1 expression can affect the enzymatic activity of MMP-9 and PLD1, we determined Western blotting to detect the protein expression of MMP-9 and PLD1. Our results showed that the anti-metastatic effect of MT-GNPs on the metastasis induced by TGF-β stimulation. Western blotting results showed that TGF-β-mediated upregulation of MMP-9 and PLD1 expression was inhibited by treatment with MT-GNPs (Figure 6B). To further investigate the promoter activity of MMP-9 and PLD1 in TGF-β-stimulated HepG2 and SK-Hep-1 cells, these cells were treated with MT extracts and MT-GNPs. Compared to cells treated with TGF-β alone, cells treated with MT extracts and MT-GNPs showed significantly suppressed MMP-9 and PLD1 promoter activity. The inhibitory effect of MT-GNPs on MMP-9 and PLD1 promoter activity was as follows: MTS-GNPs > MTR-GNPs > MTL-GNPs > MTF-GNPs (Table 3). EMT is closely correlated with metastasis in hepatocellular carcinoma. To determine the possible anti-EMT mechanism of MT-GNPs in TGF-β-stimulated HepG2 and SK-Hep-1 cells, Western blotting was used to analyze the transcription levels of E-cadherin, N-cadherin, and vimentin in hepatocellular carcinoma cells. Results showed that TGF-β-mediated upregulation of N-cadherin and vimentin expression was significantly inhibited by MT-GNPs, while TGF-β-mediated downregulation of E-cadherin expression was significantly enhanced by MT extracts and MT-GNPs (Figure 6C).

Discussion

TGF-β-induced EMT plays a role in carcinogenesis and tumor progression, resulting in the promotion of metastasis in hepatocellular carcinoma. Aberrant TGF-β signaling causes cell migration, invasion, and metastasis by generating master regulators of EMs.[18] The currently used anti-metastatic agents are associated with several limitations such as poor water solubility, biodegradability, and bioavailability. Nanomaterial therapy is one of the most

Table 3 PLD Enzymatic Activity, MMP-9, MMP-9 Promoter Activity of MTR, MTS, MTL and MTF-GNPs

Cells	PLD Activity (% of Control)		MMP-9 Relative Luciferase Activity (Fold)		PLD-1 Relative Luciferase Activity (Fold)	
	HepG2	SK-Hep-1	HepG2	SK-Hep-1	HepG2	SK-Hep-1
Control	**100**	**100**	**1**	**1**	**1**	**1**
TGF-β	271.7 ± 10.8	211.4 ± 12.1	3.5 ± 0.2	2.7 ± 0.1	5.5 ± 0.1	5.2 ± 0.5
MTR + TGF-β	208.3 ± 14.0*	163.9 ± 11.7**	2.7 ± 0.3	2.1 ± 0.1*	4.1 ± 0.3*	4.1 ± 0.4*
MTR-GNP + TGF-β	137.1 ± 6.68**	112.4 ± 2.9**	1.7 ± 0.1**	1.4 ± 0.1**	2.6 ± 0.4*	2.8 ± 0.2**
MTS + TGF-β	199.0 ± 14.6*	151.7 ± 9.7**	2.5 ± 0.2*	1.9 ± 0.2*	3.9 ± 0.4*	3.9 ± 0.2*
MTS-GNP + TGF-β	133.2 ± 8.0**	105.9 ±3.3**	1.6 ± 0.1**	1.4 ± 0.1**	2.9 ± 0.2*	2.4 ± 0.1**
MTL + TGF-β	223.5 ± 13.1*	171.0 ± 10.3**	2.9 ± 0.2	2.2 ± 0.2*	5.0 ± 0.2	4.3 ± 0.1
MTL-GNP + TGF-β	187.8 ± 7.4**	150.1 ± 5.8**	2.2 ± 0.1**	1.7 ± 0.2**	4.2 ± 0.2*	3.4 ± 0.2*
MTF + TGF-β	211.3 ± 11.7*	172.2 ± 7.6**	2.7 ± 0.3	2.4 ± 0.3	4.7 ± 0.2	4.2 ± 0.4
MTF-GNP + TGF-β	188.5 ± 5.8**	150.4 ± 4.6**	2.2 ± 0.1*	1.9 ± 0.2**	4.2 ± 0.1*	3.6 ± 0.5*

Notes: PLD enzymatic activity was determined by Amplex Red phospholipase D assay kit in HepG2 and SK-Hep-1 cells. *$p < 0.05$ and **$p < 0.01$ compared to the TGF-β group.

Abbreviations: TGF-β, transforming growth factor β; MMP-9, matrix metalloproteinases −9; PLD, phospholipase D; MTR-, MTS-, MTL- and MTF-GNPs, *Maclura tricuspidata* root-, stem-, leaves- and fruits-extract-gold nanoparticles.

promising approaches that is utilized to combat the aforementioned limitations.[9,10] HCC metastasis can be prevented or treated effectively by nanomaterial therapy whereby MT extracts are employed. Although the anticancer effect of medicinal plant-based GNPs has been suggested in previous studies, the role of PLD signaling and metastasis in hepatocellular carcinoma cells is not well investigated. Therefore, in this study, the anti-metastatic effects of GNPs synthesized from the roots, stems, leaves, and fruits of MT, with a focus on PLD1 and MMP-9 enzymatic activity in HepG2 and SK-Hep-1 cells were investigated.

MT is a widely used natural herbal remedy in China and Korea. It has multi-target therapeutic and pharmacological effects in carcinogenesis and tumor progression, which have been well demonstrated in the clinical. In particular, the roots and stems of MT have been used as traditional Chinese medicine for the treatment of rheumatism, boil, bruising, and gonorrhea. In Korea, its roots and stems are used as universal folk remedies against tumor progression in the last few decades.[31,32] Here, we first demonstrated the potential effect of MT extracts on the reduction, capsulation, and stabilization of GNPs. MTR, MTS, MTL, and MTF extracts were shown to have high phenol and flavonoid contents as well as a powerful reducing capacity, and antioxidant activity. Reaction parameters for optimizing GNPs, such as MTR, MTS, MTL, and MTF extract concentration, an aqueous solution of $HAuCl_4$ concentration, and reaction times were taken into reflection to purify the GNPs in a fast and one-step manner. These quick and simple methods were positively correlated with high phenol and flavonoid contents as well as a powerful reducing capacity, and antioxidant activity. Particle size analysis of MT-GNPs using DLS showed average particle diameters of 83.7 ~ 103.6 nm, while the PDI and zeta potential values were in the range of 0.023 ~ 0.034 and –16.8 ~ 27.9 mV, respectively, demonstrating good dispersion. Particle size analysis of MT-GNPs using HR-TEM presented that the particle size was 19.6 ~ 29.7 nm with a spherical or hexagonal morphology. Due to a layer of hydration around the MT-GNPs, MT-GNP diameters assessed by DLS were larger than those assessed by HR-TEM. As reported by Kumar et al, the optimal GNP size for the highest cellular uptake is 50 nm, while 18 and 80 nm GNPs showed high uptake by cancer cells.[33] Therefore, in our study, we also obtained MT-GNPs with similar sizes and zeta potentials. The physicochemical properties of MT-GNPs were successfully studied by DLS, HR-TEM, EDS, XRD, and FT-IR. The EDS, XRD, and FT-IR spectrums exhibited expected functional groups confirming successful reduction, stabilization, and capsulation of MT extracts onto GNPs. Several studies have also revealed that photocatalytic activity may depend on the size, morphology, and crystallographic structure of the GNPs.[34,35] MT-GNP photocatalysts showed significant photocatalytic activity towards the degradation of methylene blue and rhodamine B dyes. This can be majorly attributed to the higher surface area of MT-GNPs and synergetic coordination between MT extracts and Au.

In our study, we highlighted the role of MMP-9 and PLD1 in the molecular mechanism underlying the anti-migration and -invasion properties of MTR-, MTS-, MTL-, and MTF-GNPs. MMP-9 and PLD1 are collagenase and lipases, respectively, that regulate tumor progression by regulating cancer cell migration and invasion, and are potential therapeutic targets of metastasis as they regulate the expression of the intercellular adhesion molecule, E-cadherin, and the mesenchymal markers, N-cadherin and vimentin.[20,21] This study demonstrated that TGF-β-induced migration and invasion in HepG2 and SK-Hep-1 cells increased the enzymatic activity and protein expression of MMP-9 and PLD1. Our results also revealed the anti-migration and -invasion effects of MT-GNPs on TGF-β-induced HepG2 and SK-Hep-1 cells via inhibiting the enzymatic activity and protein expression of MMP-9 and PLD1. On the contrary, E-cadherin expression was notably increased by MT-GNPs, while that of N-cadherin and vimentin was suppressed in TGF-β-stimulated HepG2 and SK-Hep-1 cells. In addition, the anti-migration and -invasion effects of MTR-GNPs and MTS-GNPs were higher than those of MTL-GNPs and MTF-GNPs. Hence, these findings contribute to the physicochemical characterization of MTR-, MTS-, MTL-, and MTF-GNPs.

Conclusion

In the present study, GNPs were synthesized by an eco-friendly protocol using extracts from different parts of MT that are used as reducing, stabilizing, and capping agents for medical purposes. The successful synthesis of MT-GNPs was confirmed by UV-Vis spectroscopy, DLS, HR-TEM, EDS, XRD, and FT-IR. Consequently, GNPs that are proven to inhibit metastasis in hepatocellular carcinoma can enhance treatment efficacy. In addition, cell migration and invasion are major steps involved in the metastasis of hepatocellular carcinoma cells. Our results demonstrated that MT-GNPs had more effective inhibitory effects than MT extracts on cell migration, invasion, MMP-9 and PLD activity, and other EMT-related proteins. Hence, our findings provide strong evidence that MT-GNPs are beneficial for the suppression of metastasis of hepatocellular carcinoma and may serve as promising therapeutic candidates.

Funding

This research was supported by the Basic Science Research Program through the National Research Foundation of Korea (NRF), which was funded by the Ministry of Education, Science, and Technology (NRF-2018R1D1A1B07047825, 2018R1D1A1B07047497 and NRF-2018R1D1A3B07047983).

Disclosure

The authors declare that the research was conducted in the absence of any commercial or financial relationships that could be construed as a potential conflict of interest and report no conflicts of interest in this work.

References

1. Siddiqi KS, Husen A. Recent advances in plant-mediated engineered gold nanoparticles and their application in biological system. *J Trace Elem Med Biol*. 2017;40:10–23. doi:10.1016/j.jtemb.2016.11.012
2. Jadhav K, Hr R, Deshpande S, et al. Phytosynthesis of gold nanoparticles: characterization, biocompatibility, and evaluation of its osteoinductive potential for application in implant dentistry. *Mater Sci Eng C Mater Biol Appl*. 2018;93:664–670. doi:10.1016/j.msec.2018.08.028
3. Chahardoli A, Karimi N, Fattahi A, Salimikia I. Biological applications of phytosynthesized gold nanoparticles using leaf extract of Dracocephalum kotschyi. *J Biomed Mater Res A*. 2019;107(3):621–630. doi:10.1002/jbm.a.36578
4. Singh J, Dutta T, Kim KH, Rawat M, Samddar P, Kumar P. 'Green' synthesis of metals and their oxide nanoparticles: applications for environmental remediation. *J Nanobiotechnology*. 2018;16(1):84. doi:10.1186/s12951-018-0408-4
5. Vijayan R, Joseph S, Mathew B. Anticancer, antimicrobial, antioxidant, and catalytic activities of green-synthesized silver and gold nanoparticles using Bauhinia purpurea leaf extract. *Bioprocess Biosyst Eng*. 2019;42(2):305–319. doi:10.1007/s00449-018-2035-8
6. Wu S, Yang X, Luo F, et al. Biosynthesis of flower-shaped Au nanoclusters with EGCG and their application for drug delivery. *J Nanobiotechnology*. 2018;16(1):90. doi:10.1186/s12951-018-0417-3
7. Onitsuka S, Hamada T, Okamura H. Preparation of antimicrobial gold and silver nanoparticles from tea leaf extracts. *Colloids Surf B Biointerfaces*. 2019;173:242–248. doi:10.1016/j.colsurfb.2018.09.055
8. Ahn EY, Hwang SJ, Choi MJ, Cho S, Lee HJ, Park Y. Upcycling of jellyfish (Nemopilema nomurai) sea wastes as highly valuable reducing agents for green synthesis of gold nanoparticles and their antitumor and anti-inflammatory activity. *Artif Cells Nanomed Biotechnol*. 2018;46(sup2):1127–1136. doi:10.1080/21691401.2018.1480490
9. Li W, Li X, Liu S, et al. Gold nanoparticles attenuate metastasis by tumor vasculature normalization and epithelial-mesenchymal transition inhibition. *Int J Nanomedicine*. 2017;12:3509–3520. doi:10.2147/IJN.S128802
10. Wu PH, Onodera Y, Ichikawa Y, et al. Targeting integrins with RGD-conjugated gold nanoparticles in radiotherapy decreases the invasive activity of breast cancer cells. *Int J Nanomedicine*. 2017;12:5069–5085. doi:10.2147/IJN.S137833
11. Chen D, Yu D, Wang X, et al. Epithelial to mesenchymal transition is involved in ethanol promoted hepatocellular carcinoma cells metastasis and stemness. *Mol Carcinog*. 2018;57(10):1358–1370. doi:10.1002/mc.22850
12. Chen J, Cao SW, Cai Z, Zheng L, Wang Q. Epithelial-mesenchymal transition phenotypes of circulating tumor cells correlate with the clinical stages and cancer metastasis in hepatocellular carcinoma patients. *Cancer Biomark*. 2017;20(4):487–498. doi:10.3233/CBM-170315
13. Cao MT, Liu HF, Liu ZG, et al. Curcumin downregulates the expression of Snail via suppressing Smad2 pathway to inhibit TGF-beta1-induced epithelial-mesenchymal transitions in hepatoma cells. *Oncotarget*. 2017;8(65):108498–108508. doi:10.18632/oncotarget.22590

14. Chen X, Zhang S, Wang Z, et al. Supervillin promotes epithelial-mesenchymal transition and metastasis of hepatocellular carcinoma in hypoxia via activation of the RhoA/ROCK-ERK/p38 pathway. *J Exp Clin Cancer Res*. 2018;37(1):128. doi:10.1186/s13046-018-0787-2
15. Fang T, Fang Y, Xu X, et al. Actinidia chinensis Planch root extract attenuates proliferation and metastasis of hepatocellular carcinoma by inhibiting epithelial-mesenchymal transition. *J Ethnopharmacol*. 2019;231:474–485. doi:10.1016/j.jep.2018.11.014
16. Padthaisong S, Thanee M, Techasen A, et al. Nimotuzumab inhibits cholangiocarcinoma cell metastasis via suppression of the epithelial-mesenchymal transition process. *Anticancer Res*. 2017;37(7):3591–3597. doi:10.21873/anticanres.11729
17. Hseu YC, Lin YC, Rajendran P, et al. Antrodia salmonea suppresses invasion and metastasis in triple-negative breast cancer cells by reversing EMT through the NF-kappaB and Wnt/beta-catenin signaling pathway. *Food Chem Toxicol*. 2019;124:219–230. doi:10.1016/j.fct.2018.12.009
18. Zhang Z, Liu T, Yu M, Li K, Li W. The plant alkaloid tetrandrine inhibits metastasis via autophagy-dependent Wnt/beta-catenin and metastatic tumor antigen 1 signaling in human liver cancer cells. *J Exp Clin Cancer Res*. 2018;37(1):1–11. doi:10.1186/s13046-018-0678-6
19. Gomez-Cambronero J, Carman GM. Thematic minireview series on phospholipase D and cancer. *J Biol Chem*. 2014;289(33):22554–22556. doi:10.1074/jbc.R114.593137
20. Roth E, Frohman MA. Proliferative and metastatic roles for phospholipase D in mouse models of cancer. *Adv Biol Regul*. 2018;67:134–140. doi:10.1016/j.jbior.2017.11.004
21. Utter M, Chakraborty S, Goren L, Feuser L, Zhu YS, Foster DA. Elevated phospholipase D activity in androgen-insensitive prostate cancer cells promotes both survival and metastatic phenotypes. *Cancer Lett*. 2018;423:28–35. doi:10.1016/j.canlet.2018.03.006
22. Boldeiu A, Simion M, Mihalache I, et al. Comparative analysis of honey and citrate stabilized gold nanoparticles: in vitro interaction with proteins and toxicity studies. *J Photochem Photobiol B*. 2019;197:111519. doi:10.1016/j.jphotobiol.2019.111519
23. Chahardoli A, Karimi N, Sadeghi F, Fattahi A. Green approach for synthesis of gold nanoparticles from Nigella arvensis leaf extract and evaluation of their antibacterial, antioxidant, cytotoxicity and catalytic activities. *Artif Cells Nanomed Biotechnol*. 2018;46(3):579–588. doi:10.1080/21691401.2017.1332634
24. Dhayalan M, Denison MIJ, Ayyar M, Gandhi NN, Krishnan K, Abdulhadi B. Biogenic synthesis, characterization of gold and silver nanoparticles from Coleus forskohlii and their clinical importance. *J Photochem Photobiol B*. 2018;183:251–257. doi:10.1016/j.jphotobiol.2018.04.042
25. Park SY, Yi EH, Kim Y, Park G. Anti-neuroinflammatory effects of Ephedra sinica Stapf extract-capped gold nanoparticles in microglia. *Int J Nanomedicine*. 2019;14:2861–2877. doi:10.2147/IJN.S195218
26. Hiep NT, Kwon J, Hong S, et al. Enantiomeric isoflavones with neuroprotective activities from the Fruits of Maclura tricuspidata. *Sci Rep*. 2019;9(1):1757. doi:10.1038/s41598-018-36095-8
27. Jeon SM, Lee DS, Jeong GS. Cudraticusxanthone A isolated from the roots of Cudrania tricuspidata inhibits metastasis and induces apoptosis in breast cancer cells. *J Ethnopharmacol*. 2016;194:57–62. doi:10.1016/j.jep.2016.08.042
28. You Y, Min S, Lee YH, Hwang K, Jun W. Hepatoprotective effect of 10% ethanolic extract from Curdrania tricuspidata leaves against ethanol-induced oxidative stress through suppression of CYP2E1. *Food Chem Toxicol*. 2017;108(Pt A):298–304. doi:10.1016/j.fct.2017.08.007
29. Kim OK, Jun W, Lee J. Effect of Cudrania tricuspidata and Kaempferol in endoplasmic reticulum stress-induced inflammation and Hepatic Insulin resistance in HepG2 Cells. *Nutrients*. 2016;8(1):60. doi:10.3390/nu8010060
30. Mocan A, Zengin G, Mollica A, et al. Biological effects and chemical characterization of Iris schachtii Markgr. extracts: A new source of bioactive constituents. *Food Chem Toxicol*. 2018;112:448–457. doi:10.1016/j.fct.2017.08.004
31. Jo YH, Kim SB, Liu Q, Do SG, Hwang BY, Lee MK. Comparison of pancreatic lipase inhibitory isoflavonoids from unripe and ripe fruits of Cudrania tricuspidata. *PLoS One*. 2017;12(3):e0172069. doi:10.1371/journal.pone.0172069
32. Kim DW, Lee WJ, Asmelash Gebru Y, et al. Comparison of bioactive compounds and antioxidant activities of maclura tricuspidata fruit extracts at different maturity stages. *Molecules*. 2019;24(3). doi:10.3390/molecules24030567
33. Kumar D, Mutreja I, Chitcholtan K, Sykes P. Cytotoxicity and cellular uptake of different sized gold nanoparticles in ovarian cancer cells. *Nanotechnology*. 2017;28(47):475101–6528/aa935e. doi:10.1088/1361-6528/aa935e
34. Baruah D, Goswami M, Yadav RNS, Yadav A, Das AM. Biogenic synthesis of gold nanoparticles and their application in photocatalytic degradation of toxic dyes. *J Photochem Photobiol B*. 2018;186:51–58. doi:10.1016/j.jphotobiol.2018.07.002
35. Choudhary BC, Paul D, Gupta T, et al. Photocatalytic reduction of organic pollutant under visible light by green route synthesized gold nanoparticles. *J Environ Sci*. 2017;55:236–246. doi:10.1016/j.jes.2016.05.044